

www.acsanm.org Article

Carrier Dynamics of CsPbBr₃ Perovskite Nanocrystals from Ensemble Average to Single-Particle Level for Safeguarding the Dilution-Induced Excited-State Decay Heterogeneity

N. V. S. Praneeth, Shovon Chatterjee, Subarna Biswas, Amitrajit Mukherjee, Ram Sewak, Abhijit Dutta, Anirban Mondal, Saumyakanti Khatua, and Nimai Mishra



Cite This: ACS Appl. Nano Mater. 2025, 8, 20726-20737



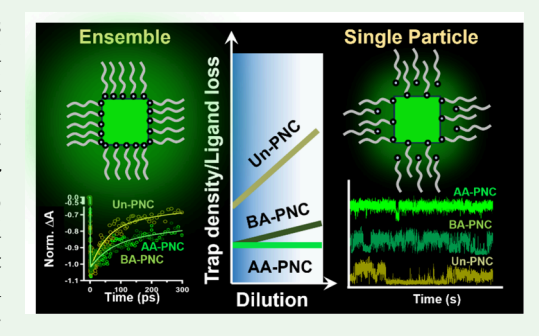
ACCESS I

III Metrics & More

Article Recommendations

Supporting Information

ABSTRACT: Photoluminescence blinking remains one of the main challenges for perovskite nanocrystals (PNCs) to be used in single-emitter devices and light-emitting diodes. Besides the persistent surface traps, dilution-induced ligand desorption also affects the blinking. The ligands that can passivate the surface without affecting the charge-transfer efficiency and can resist the dilution-induced desorption will be ideal for having a blinking-free/suppressed PNC for device applications. We used ascorbic acid (AA) and benzoic acid (BA), two short-chain ligands, in the postmodification of oleic acid/oleylamine capped PNC (Un-PNC). The ensemble average transient absorption study reveals that both AA and BA reduced the surface trapping contribution to 12 from 28% in Un-PNC. However, the single-particle photoluminescence analysis reveals AA-PNC to be superior with 84% photoluminescence ON-fraction, 10%, and 23%



more compared to BA-PNC and Un-PNC, respectively. A similar trend was observed for AA-PNC in the electron-trapping rate, with a 5-fold and 20-fold reduction than Un-PNCs and BA-PNCs, respectively. AA-PNCs also maintained long-term stability under ambient conditions with a minute decrease in the time-averaged ON-fraction by 9.5% after 4 months, whereas Un-PNCs showed a 36% reduction. Time-resolved photoluminescence and simulation suggest that the dilution-induced ligand detachment due to weaker binding affinity of BA compared to AA with the PNC surface is found to be the origin of disparity in blinking despite having similar photophysics in the bulk spectroscopic analysis. Mitigating the dilution-induced heterogeneity, AA is found to be an effective ligand for synthesizing blinking-suppressed PNCs without compromising charge transfer, opening a pathway for potential application in bioimaging, single-emitter devices, and LEDs.

KEYWORDS: short-chain acid treatment, trap passivation, carrier trapping rate, transient absorption spectroscopy and single-particle photoluminescence microscopy, perovskite nanocrystals

1. INTRODUCTION

Cesium-lead halide perovskite (CsPbX3; X is Cl, Br, and I) nanocrystals (PNCs) hold tremendous potential in optoelectronic and photocatalytic applications. ^{1–3} Their high absorption coefficient and high photoluminescence (PL) yield make them ideal candidates for LED and display applications. 1,4,5 Although they are known to be more defect-tolerant compared to conventional quantum dots, they still suffer from surface traps caused by inadequate ligand passivation.⁶ The commonly used oleic acid (OA)-oleylamine (OAm) ligand pair is vulnerable in colloidal conditions due to the dynamic capping that results in ligand loss over time.^{6,7} This leads to the formation of vacant sites, which act as shallow charge-carrier traps.8 Also, the hot-injection synthetic condition is responsible for forming halide vacancies on the PNC surface, which eventually act as carrier trapping centers. After photoexcitation, the charged carriers fall into these traps, and some part of it relaxes through nonradiative (NR) recombination.^{8,9}

This becomes more severe when the NC surface trap density increases. ^{10,11} These traps adversely affect the PLQY and carrier lifetime, which can be observed through bulk-level steady-state and time-resolved (TR) spectroscopic measurements. ¹¹

On the other hand, at single-particle (SP) concentrations, the participation of trap states in the carrier recombination process leads to PL intermittency between the bright (ON) state and the dark (OFF) state, commonly termed PL blinking. This intermittency in their PL signal limits their practical applications in areas where continuous emission

Received: July 7, 2025
Revised: October 8, 2025
Accepted: October 10, 2025
Published: October 22, 2025





Scheme 1. Schematic Representation of AA and BA Treatment on Pristine CsPbBr₃ Nanocrystals (Un-PNCs)

is needed to track any process or in display applications. 15,16 PL blinking can be classified into several categories depending on the nature of the traps involved in the carrier recombination.¹⁶ A charged carrier can get trapped in a shallow surface trap and then recombine nonradiatively before another excitation cycle can take place. Such an NR process leads to temporal PL fluctuation known as NR band edge carrier (NBC) blinking or type-C blinking. 12,16 On the other hand, the longer time tapping makes the NC charged, leading to the formation of a trion upon absorbing another photon. This trion can subsequently relax through NR Auger recombination or radiatively with almost twice the exciton recombination rate. The temporal PL fluctuation arising from this trion relaxation involving long-lived trap states is termed AC blinking. 16 Another NR process (type-B blinking) involves hot carriers (HCs) directly being trapped in defects. Their temporal average lifetime staying unaffected by PL intensity blinking originating from the HC trapping and remaining constant throughout is known as HC blinking.¹⁷ For the PNC, it has already been observed by several research groups that temporal PL fluctuation is contributed either by NBC, AC, or HC blinking. In some cases, it has also been found that either two of these mechanisms are responsible for the PL intermittency. 18,19 The energetic distribution of trap states mediated by the spatial inhomogeneity of the local environment mainly dictates the PL blinking mechanism in PNCs. 16

Over the past few years, various surface treatment methods have been developed to reduce the trap density in CsPbBr₃.²⁰⁻²³ Among them, postsynthesis surface passivation with small molecules with better chelating affinity than OA/ OAm is quite popular due to easy synthesis protocols. A sizable number of such molecules have been reported to have successfully reduced trap densities and improved colloidal stability at bulk PNC concentrations, resulting in an improved PLQY reaching almost unity. However, only a few studies probed the effect of the varying ligand chemistry on the PL intermittencies of CsPbBr3 at SP concentrations. In principle, the bulk studies are expected to be consistent with SP measurements because bulk measurement represents the ensemble average of individual particle measurements. However, significant differences may arise for some passivating molecules/ligands as they usually bind weakly with the CsPbBr3 surface via van der Waals and/or electrostatic interactions. The equilibrium between the bound and unbound ligands may lead to ligand removal from the CsPbBr3 surface during the dilution process required for SP sample preparation. This eventually yields inferior performance at SP concentrations.²⁴ Therefore, the effectiveness of the surface passivating molecules/ligands should be assessed at both bulk and SP concentrations. Most importantly, for device applications, the ligand molecules need to effectively facilitate charge transfer from the NCs. The long-chain ligands may

limit this charge-transfer process due to the formation of the insulating layer around the NC, despite being effective in colloidal stability and surface passivation and consequently suppressing PL intermittency. The short-chain ligand that can resist the dilution-induced ligand desorption, thus, may be an ideal option for getting blinking-suppressed NC. Earlier, short-chain benzoic acid (BA) and ascorbic acid (AA) have shown significant improvement in the bulk PL properties and colloidal stability. The charge-transfer properties have also been significantly enhanced by using these short-chain ligand systems. The effectiveness of these two short-chain ligands throughout different concentration regimes is yet to be explored to testify to their passivating strength.

Here, we investigated the effect of short-chain BA and AA treatments on the CsPbBr3 NC surface across a broad PNC concentration range using transient absorption (TA) spectroscopy and SPPL microscopy. Our TA and SPPL microscopy revealed enhanced optical properties of CsPbBr3 nanocrystals following BA and AA passivation. However, the effectiveness of BA and AA differed significantly. A similar extent of trap passivation by both AA and BA was observed from the chargecarrier dynamics at the ensemble level, as probed through TA spectroscopy. The SPPL blinking study, on the other hand, indicated that AA molecules were significantly more effective than BA in passivating surface traps. The average carrier trapping rate recorded on ~75 PNCs from their truncated power law fitting parameters showed that purified CsPbBr₃ NCs (Un-PNCs) had a trapping rate of 11.83 s⁻¹, improving to 3.05 s⁻¹ for BA-treated PNCs and further improving to 0.53 s⁻¹ for AA-treated ones. Further, AA passivation demonstrated substantially better long-term stability, with AA-PNCs exhibiting the least degradation in NC quality and a minor change in their ON-fraction time from 0.85 to 0.77 after 4 months. Through additional dilution-dependent TRPL studies, we hypothesized that the inferior performance of BA resulted from a weaker binding affinity for CsPbBr3 nanocrystals, making them more likely to detach during the dilution process required for SPPL microscopy. This hypothesis was further supported by DFT calculations using VASP, 28,29 which revealed that the adsorption energy of AA post-treated PNCs is significantly less negative than that of BA, making BA more prone to detaching from the PNC surface under dilution. Our study provides a detailed understanding of the effect of shortchain ligands (BA and AA) on the carrier recombination process in PNCs, from ensemble average to single NC level. This study also demonstrates that we can achieve long-term stable blinking-suppressed PNCs by safeguarding the dilutioninduced excited-state heterogeneity through the use of AA. This paves the way for their use as highly efficient LEDs and single-emitter devices.

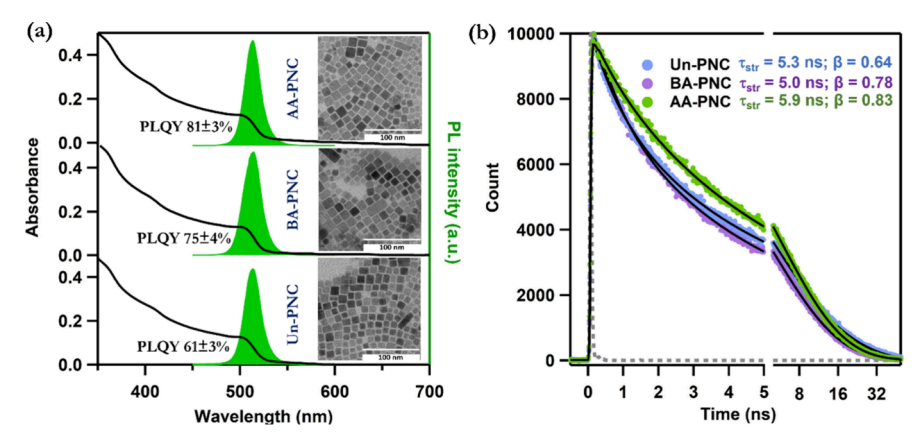


Figure 1. Optical properties of the Un-CPB and the treated NCs. (a) Steady-state absorption and PL spectra of Un-PNC, BA-PNC, and AA-PNC. Corresponding TEM images are given in the inset. (b) Time-resolved PL of Un-PNC, BA-PNC, and AA-PNC with stretched exponent fitting parameters. Excitation wavelength 405 nm; IRF 85 ps

2. RESULTS AND DISCUSSION

2.1. Material and Optical Characterizations. The CsPbBr₃ NCs were synthesized using our previously used protocol through hot injection without inert atmospheric conditions.²⁵ According to our previous reports, the postsynthetic treatment with BA and AA was done by adding the requisite amount of respective acids to the colloidal solution of as-synthesized purified NCs. 25,26 The NC synthesis and postsynthetic treatment are schematically shown in Scheme 1, and the details are documented in Section S1 of the Supporting Information (SI). The purified CsPbBr₃ NCs are termed Un-PNCs, whereas the BA- and AA-treated NCs are termed BA-PNCs and AA-PNCs, respectively. Un-PNCs show a broad characteristic absorption with a band edge near 506 nm and a sharp PL centered at 512 nm with a PLQY of 61 \pm 3% (lower panel of Figure 1a). Transmission electron microscopy (TEM) image Un-PNCs shows a homogeneous size distribution with an average size of 11.5 nm (inset of the lower panel of Figures 1a and S3). The Un-PNC crystallizes in the orthorhombic phase, confirmed by the powder X-ray diffraction pattern (Figure S3).²⁶ The postsynthetic treatment with BA and AA does not alter the size distribution, crystal phase, absorption band edge, and PL position (Figures 1a, S3, and S4). However, following BA and AA treatment, the PLQY of the NCs enhanced to 76 \pm 4% and 81 \pm 3%, respectively, suggesting suppression of the nonradiative process associated with the trap states (Figure 1a).

TRPL spectroscopy was performed to observe the change in the exciton decay dynamics associated with the amplification of the PLQY upon BA and AA treatment on Un-PNCs. The TRPL decay kinetics of Un-PNCs and the treated NCs have been fitted with the stretched exponential fitting equation. The physical basis of using a stretched exponential fitting function $\exp[-(t/\tau)^{\beta}]$ for the perovskite NCs can be explained through the heterogeneity in the PL decay dynamics of NCs. 30,31 The heterogeneity in the PL decay dynamics may have two basic origins. Primarily, it can be a result of the size distribution that can affect the distribution of the excited-state lifetime. Another main reason for this heterogeneity can be a result of the distribution in the trapping and detrapping rates from the energetically distributed trap states. 31 β is the stretched exponent and can have a value between 1 and 0.31,32 The deviation of the value of β from unity signifies the increased trap density distribution for a particular NC.³¹ The Un-PNC

shows a stretched average lifetime of 5.3 ns with a β of 0.64 (Figure 1b and Table S1). Upon treatment with BA, the stretched lifetime is estimated to be 5.0 ns, and β increased to 0.78, suggesting the reduced trap density distribution through passivation of surface traps (Figure 1b and Table S1) as the size distribution remains unchanged after the treatment (Figure S3), whereas in AA treatment, both stretched lifetime and β values increase and reach 5.9 ns and 0.83, respectively (Figure 1b and Table S1). This further suggests that the AA treatment effectively reduces the trap density distribution through proper surface passivation and is more effective than BA.

2.2. Ultrafast Carrier Dynamics. We performed femtosecond TA spectroscopy to monitor the detailed effect of short acid ligand incorporation on the charge-carrier dynamics of CsPbBr₃ NCs. The NCs were excited above the band gap at 400 nm by a femtosecond pulsed laser. The fluence was kept at 3.8 μ J cm⁻². The exciton density $\langle N \rangle$ is calculated to be 1.15, indicating the formation of possible multiexciton species (Section S1.11). All three samples (Un-PNC, BA-PNC, and AA-PNC) show a strong ground-state bleach (GSB) signal near the band edge position (~504 nm), which is in line with the previous studies (Figure S5) (early time up to 5 ps and later time from 5 to 1500 ps, respectively; Figure S5d-f and g-i, respectively).33,34 At an early time (<5 ps), a strong excited-state absorption (ESA) band appears for all samples at around ~520 nm, attributed to the biexciton effect (Figure S5a-f).34,35 This biexciton effect originates from the Coulombic interaction between the hot exciton produced by the pump and the band edge exciton produced by the probe pulse. This ESA band is short-lived and disappears after HC cooling. To have an understanding of the excited-state processes, the GSB signals of all three samples were fitted with a triexponential fitting function. All GSB bands show a rise time due to excitonic state filling originating from the HC cooling process (Figure 2a). 34,36,37 The HC cooling process of Un-PNC is estimated to be 722 fs (Figure 2a and Table S2). After treating with AA and BA, this cooling time was modified to 912 and 864 fs, respectively (Figure 2a and Table S2). This slightly slower cooling time of the treated samples may be attributed to the passivation of the trapping sites, which allows the direct quenching of the HCs.³⁸ Following the formation, the GSB decay kinetics show two different time constants, which are tabulated in Table S2. Although following the

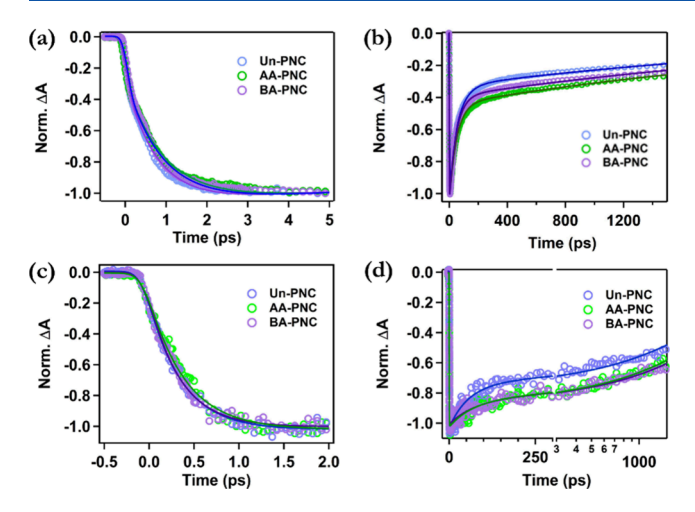


Figure 2. Kinetics of the GSB bands from ultrafast TA spectroscopy. (a) GSB formation kinetics of Un-PNC, AA-PNC, and BA-PNC at exciton density $\langle N \rangle = 1.15$. (b) GSB decay kinetics of Un-PNC, AA-PNC, and BA-PNC at exciton density $\langle N \rangle = 1.15$. (c) GSB formation kinetics of Un-PNC, AA-PNC, and BA-PNC at exciton density $\langle N \rangle = 0.24$. (d) GSB decay kinetics of Un-PNC, AA-PNC, and BA-PNC at exciton density $\langle N \rangle = 0.24$. The excitation wavelength is 400 nm.

literature, we have performed the experiment in low excitation fluence (3.9 μ J cm⁻²; $\langle N \rangle$ = 1.15),³⁹ a short time constant of ~50 ps appears along with the single-exciton recombination process (>1.5 ns) (Figure 2b). The ~50 ps time component resembles the biexcitonic recombination process.^{40,41} From the decay kinetics of the three samples, it is evident that Un-PNC shows the fastest recovery, followed by BA-PNC and AA-PNC.

Also, interestingly, Un-PNC shows almost 67% recovery through the process corresponding to the ~50 ps time constant, whereas AA-PNC and BA-PNC recovery through this process is 58 and 63%, respectively. In many cases, it is reported that the trapping process of the excitons also occurs on a similar time scale.³⁴ So, it is possible that some trapping process may be contributing to the recovery of the GSB, which apparently increases the amplitude of the short-time component. Here, to confirm the possibility of the contribution of the trapping process in the GSB recovery, we have further experimented with comparatively much lower excitation fluence (0.8 μ J cm⁻²; $\langle N \rangle$ = 0.24).

The spectral features, exciting all three samples at a relatively lower excitation fluence of 0.8 μ J cm⁻² ($\langle N \rangle$ = 0.24), are depicted in Figure S6 (early time up to 1.5 ps and later time from 2 to 1500 ps, respectively; Figure S6d-f and g-i, respectively). The early time GSB formation due to the HC cooling process becomes much faster for all of the samples due to the minimization of the HC bottleneck effect (Figure 2c). The Un-PNC and both treated samples show almost similar HC cooling times, indicating that the effect of short-chain acid ligand passivation has no significant impact on the HC cooling dynamics, and the little variation of the cooling time at higher excitation fluence may originate from some other effect or artifact (Table S3). However, the GSB decay kinetics shows a slower recovery at this excitation fluence (Figure 2d). The GSB recovery for all three samples shows two time constants (Table S3). The longer time constant of >1.5 ns is attributed to the exciton recombination process. The untreated and treated samples also show a faster decay time of ~60 ps. The contribution of this faster component in the GSB recovery of

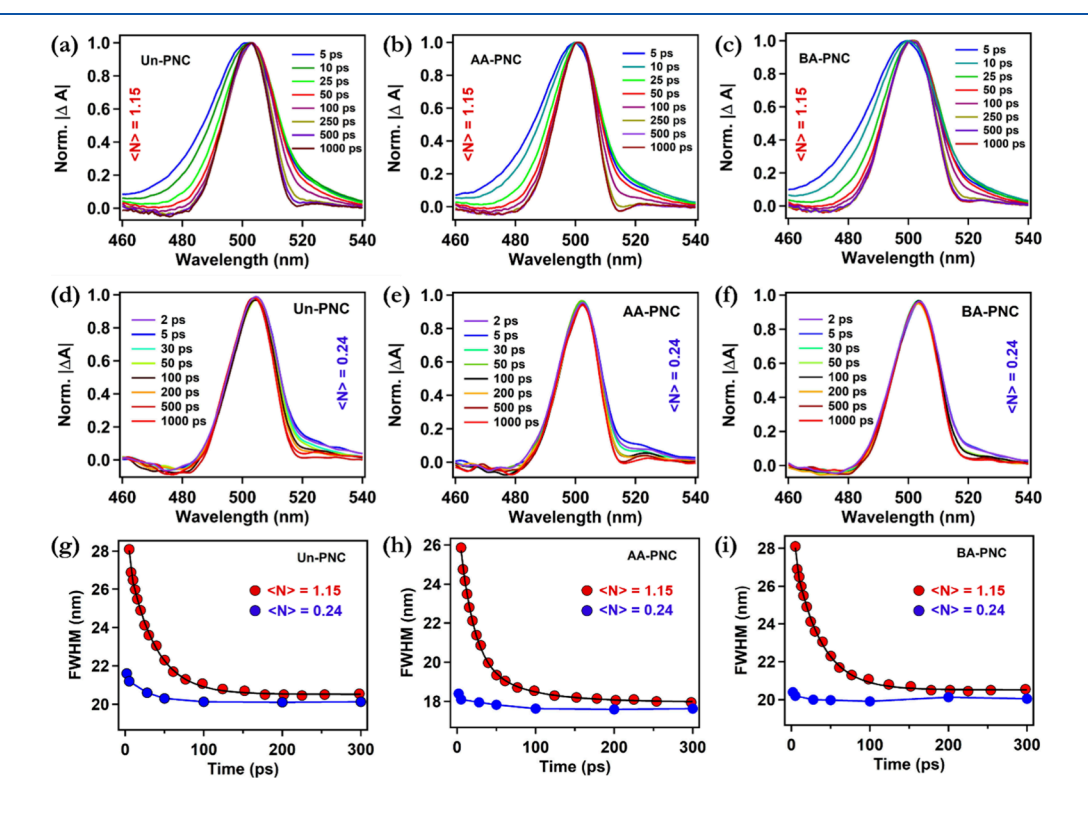


Figure 3. Normalized TA spectra (5–1000 ps) of (a) Un-PNC, (b) AA-PNC, and (c) BA-PNC at an exciton density $\langle N \rangle = 1.15$. Normalized TA spectra (2–1000 ps) of (d) Un-PNC, (e) AA-PNC, and (f) BA-PNC at an exciton density $\langle N \rangle = 0.24$. The time-dependent change in fwhm of the GSB bands of (g) Un-PNC, (h) AA-PNC, and (i) BA-PNC at exciton density $\langle N \rangle = 1.15$ (red circles) and exciton density $\langle N \rangle = 0.24$ (blue circles), pump fluence. The black curves through red circles correspond to the respective exponential fitting.

Un-PNC is 28%, whereas for AA-PNC and BA-PNC, the relative contribution of this process reduces to 12 and 13%, respectively. At very low excitation fluence, as the possibility of the multiexciton process is almost zero, this faster time constant may be attributed to the trapping of the charge carriers to the band edge surface states. This also indicates that the trapping contribution is higher in Un-PNC than in the treated samples. However, although the possibility of any multiexciton generation is almost impossible at this low photon density, we further analyzed the TA spectra of the untreated and treated samples to reconfirm whether these ~60 ps components arise solely due to the trapping process. Further, to confirm the origin of short time constants in two different fluences, a global analysis is done on Un-PNC (Figure S7). The decay-associated spectra (DAS) of Un-PNC show three components at both fluences, consistent with our analysis. The DAS associated with the shortest time constants (0.35 ps at $\langle N \rangle$ = 0.24, and 0.8 ps at $\langle N \rangle$ = 1.15) show a derivative nature, originating from the Coulombic interaction between the hot exciton and the band edge exciton.³⁴ This is the origin of the ESA band observed at early times below the band edge as discussed earlier. Also, the DAS of >1500 ps components is associated with the single exciton at 504 nm. At a lower excitation fluence of $\langle N \rangle = 0.24$, the DAS of ~60 ps component are found to be red-shifted from the exciton bleach and observed at 509 nm (Figure S7a), whereas at higher excitation fluence of $\langle N \rangle$ = 1.15, the DAS of the ~50 ps component show a much broader feature with its maxima at 498 nm (Figure S7b). This further confirms that the origins of the two short components are different at two different excitation fluences. The shallow traps are found in CsPbBr₃ just below the band edge, on the lower energy side than the exciton, indicating that the origin of the ~60 ps component at lower excitation fluence is shallow traps, and the biexciton species is generally found energetically higher than the exciton. 42 This further suggests that the ~50 ps component at higher excitation fluence mainly originates from biexciton formation. However, at higher fluence, the trapping also contributes, but the extent is much lower than that of the biexciton species. This is why, through DAS analysis, we could not separate these two very similar time constants.

The normalized TA spectra of Un-PNC, AA-PNC, and BA-PNC at $\langle N \rangle = 1.15$ are depicted in Figure 3a-c, respectively. The normalized TA spectra have been shown from 5 ps to avoid the HC contribution to the spectral feature of the respective NCs. At an early time, the broadening spectral feature of the GSB band of all samples at high excitation fluence originates due to the presence of the biexciton, whereas at low excitation fluence ($\langle N \rangle = 0.24$), the normalized TA spectra of Un-PNC, AA-PNC, and BA-PNC show minimal spectral broadening of the GSB band at an early time (Figure 3d,e). The time-dependent change of this GSB spectral feature for each sample at two different excitation pump fluences is analyzed by the time-dependent change in the full width at half-maximum (fwhm) of the respective spectra (Figure 3g-i). At high excitation pump fluence ($\langle N \rangle = 1.15$), the fwhm for Un-PNC changes from 28.2 to 20.6 nm (Figure 3g). Similarly, AA-PNC and BA-PNC show the shrinkage of the fwhm of their GSB bands from 26 to 18.2 nm and 28.1 to 20.7 nm, respectively (Figure 3h,i, respectively). The broadening of the GSB at an early time was predominantly observed at the higher energy side of the exciton bleach signal, indicating the presence of the biexciton. Also, at the lower excitation fluence ($\langle N \rangle$ =

0.24), all three samples show very small changes in their GSB fwhm, which are plotted along with their respective high excitation fluence change (Figure 3g–i). The very small change in the fwhm at this lower fluence is observed mainly on the lower energy side of the excitonic bleach, indicating the trapping process. This confirms the absence of a biexciton at the low fluence and the short time constant of ~ 60 ps originating from the trapping of the excitons. This trapping process is found to be maximum for Un-PNC, indicating a higher trap density. After treatment with both AA and BA, the decay kinetics indicates the suppression of the trapping process, which slows the GSB recovery.

Further, the time-dependent shrinkage of the fwhm of all three samples was fitted with the exponential decay function. The Un-PNC shows a decay time of 33 ps, whereas the AA-PNC and BA-PNC show the decay at 29 and 31 ps, respectively. This time constant of ~30 ps is very similar to that of the biexcitonic recombination process (~50 ps). However, it is already been discussed that the ~50 ps time constant at 3.9 μ J cm⁻² pump fluence ($\langle N \rangle = 1.15$) has the trapping contribution with the biexciton recombination, which is the reason for the deviation in the time constant. Now, to estimate the exact biexciton recombination time for all three samples, we have subtracted the GSB recovery kinetics at high fluence from the GSB recovery kinetics at low fluence. The subtracted kinetics is depicted in Figure S8, which is exponentially fitted, producing biexciton recombination times of 29, 31, and 34 ps for Un-PNC, AA-PNC, and BA-PNC, respectively. These extracted biexciton recombination times are exactly similar to the decay kinetics of the fwhm for all of the samples. This further confirms that the time-dependent change in the fwhm of the GSB band is associated with the biexciton decay kinetics, and the change in the surface does not have any impact on the biexciton decay dynamics.

2.3. Single-Particle PL Blinking Study. The comparative analysis of the charge-carrier dynamics of BA-PNC, AA-PNC, and Un-PNC makes it clear that the surface traps can be successfully passivated by AA and BA treatments. This ensemble average view of carrier dynamics, however, is inadequate to reveal the characteristics of the traps. The PL blinking investigation has been conducted on individual NCs to help understand the type of traps involved in the carrier recombination process in Un-PNC and how AA and BA treatment affects it.

The SP microscopy and spectroscopy study of spatially wellseparated PNCs was carried out on a confocal microscope (optical path in Figure S1 and imaging procedure are detailed in Section S1.13, SI) using 405 nm CW and 485 nm picosecond pulsed laser, keeping the excitation power density at $\sim 10 \text{ W/cm}^2$. Figure 4a,c,e shows the confocal PL images of Un-PNC, BA-PNC, and AA-PNC, respectively. The diffraction-limited spots in the PL images belong to the respective PNC, and not an artifact was confirmed from their respective PL spectrum (inset of the respective Figures) and their corresponding PL intensity timetrace and occurrence histogram (Figure 4b,d,f) for Un-PNC (top), BA-PNC (middle), and AA-PNC (bottom), respectively. The corresponding zoomed timetraces and their respective dwell times are given in Figure S9. Zoomed timetraces for Un-PNC, BA were taken to ascertain that all PL spots are not artifact, PL spectrum of all spots in each image were taken, and the same slide was used to record their spatial distribution from AFM (Figure S2).

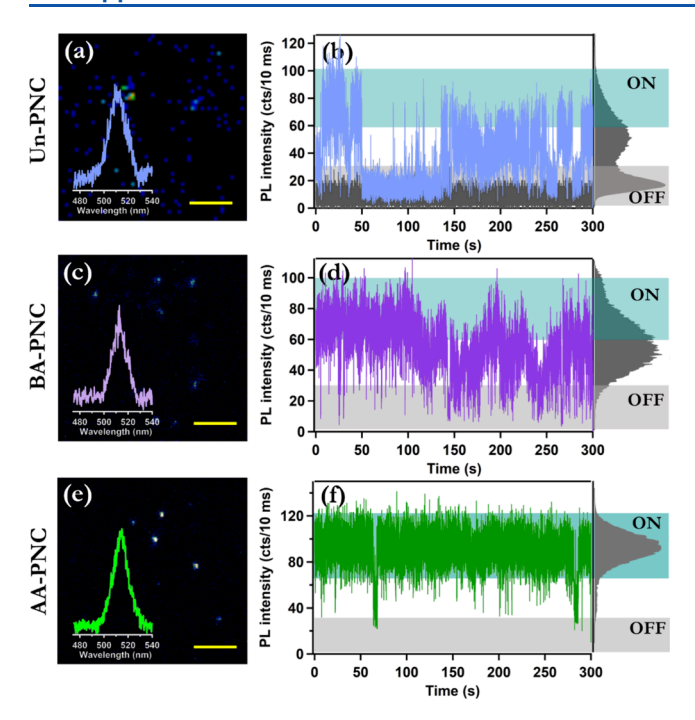


Figure 4. (a,c,e) PL image (scale bar 2.0 μ m) and PL spectra of a SP (inset). (b,d,f) PL intensity timetrace and its histogram (shaded for intensities of different states) of a SP for each PNC system.

PL intensity timetrace examination shows that the UN-PNCs have temporal behavior transitioning between various intensity levels with a significantly high fraction of OFF-state (Figure 4b). Using general parlance, most particles showed 'Blinking Up' and 'Frequently Blinking' type intermittency, with OFF states lasting from a few tens of milliseconds to some seconds (Figures 4b and S10).⁴³ This diversity of intensities leads to broadening of the intensity histogram with multiple overlapping Gaussians. Such intermittency is considerably suppressed in BA-PNCs, where the majority of intensities are observed several times above the background with one single ON-state Gaussian and very few gray and OFF intensity levels (Figure 4d). Other timetraces of BA-PNC recorded at different bin times are given in Figure S11. In the case of AA-PNCs, it was found that the OFF-state is significantly suppressed by AA passivation with particles present in 'mostly ON' condition. Such timetraces are also referred to as 'Blinking Down' where the emitter continuously emits photons which intermittently stop but quickly return to emitting levels, as shown in Figure 4f. Other timetraces recorded at different "bin time" are given in Figure S12 showing a similar trend in temporal PL behavior.

PL intermittency was statistically quantified by applying the bin and threshold' method looking at their dwell times in ON, OFF, and/or gray state and their corresponding probability density function (PDF). Hershold for ON events was taken as all intensities above background $+6\sigma_{\rm BG}$ ($I_{\rm ave,BG}$ + $6\sigma_{\rm BG}$), intensities below the average background signal $+3\sigma_{\rm BG}$ ($I_{\rm ave,BG}$ + $3\sigma_{\rm BG}$) were taken as OFF events, and everything in between assigned as gray events, with σ being the standard deviation of background timetrace. ON, OFF, and/or gray event (N) dwell times for traces in Figure 4 and their zoomed timetraces are given in Figure S9 (top and middle panel). Corresponding PDF was calculated using eq 1, and the normalized PDF of ON-state for all three PNCs is given in Figure Sa, and each timetrace was observed to follow a

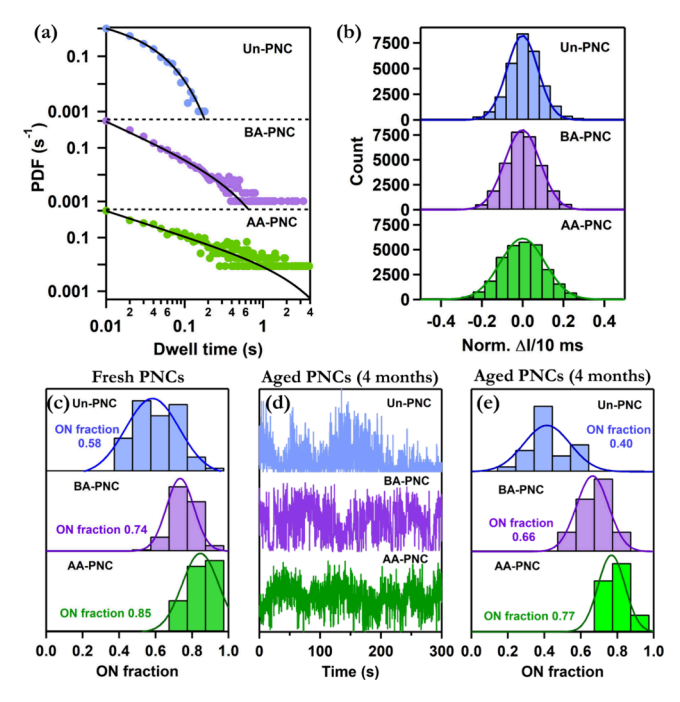


Figure 5. (a) ON-state probability density, (b) one-frame jump distribution for all fraction of fresh PNCs of all three PNC system, (c) ON events fraction statistics for 72 fresh PNCs, (d) timetrace of 4 month old PNCs, and (e) ON events fraction of 4 months old (4M) PNCs.

truncated power law as given in eq 2 below (solid line fits with same color code). The truncated power law contains a power law function observed at lower dwell times and an exponential decay behavior at higher dwell times. OFF and gray state PDF for each timetrace in Figure 4 is given along with their dwell time distribution in Figure S9 (bottom panel) and are seen to follow a power law distribution as well. Power law exponent a_i indicating the probability to switch from the i^{th} state to the other is indicative of the characteristic of PL intermittency; the smaller the m_i is, the lesser the probability to switch, and more probable that it is found mostly in the i^{th} state. Statistics in Table 1 shows that the m_{on} for AA-PNC is the lowest followed

Table 1. Statistics of PDF Fitting for 50 PNCs

samples	trapping rate $[k_{on}](s^{-1})$	$m_{ m on}$	$m_{ m off/gray}$
Un-PNC	11.83 (±3.21)	1.22 (±0.07)	$1.29 \ (\pm 0.17)$
BA-PNC	$3.05 (\pm 1.70)$	1.26 (±0.11)	$1.34 \ (\pm 0.23)$
AA-PNC	$0.53 (\pm 0.16)$	$1.03 \ (\pm 0.09)$	1.86 (±0.19)

by Un-PNC and BA-PNC, indicating that AA passivation leads to significant improvement in the temporal PL behavior of PNCs vis-a-vis ON-state characteristic. Considerably better values of Un-PNC indicate that these samples are fairly defect-tolerant in pristine form with mainly a shallow trap-mediated nonradiative relaxation pathway. Also, $k_{\rm on}$ of TRPL indicative of carrier trapping rate by NBC shallow traps show a marked trend of AA \ll BA < Un with values of 0.46, 3.14, and 11.75 s⁻¹ for the given timetraces in Figure 4, indicative of significant passivation of trap sites upon AA treatment. This observation was further supported by statistical analysis on 76 PNCs (Table 1), which shows that AA passivation resulted in \sim 20 times and \sim 4 times reduction in the carrier trapping rate compared to Un-PNCs and BA-treated PNCs, respectively.

Although trapping and detrapping rate studies are focused on electron trapping only, hole trapping is also possible in PNCs. However, a similar reduced mass of electrons and holes in PNCs makes it extremely difficult to distinguish them from spectroscopy study. Therefore, we refer to carrier trapping without specifying if electrons are trapped or holes are trapped (eqs 1-3).

$$P_i(t) = N_i(t) / (N_{\text{total},i} \times \Delta t_{\text{avg},i})$$
 (1)

$$P_i(t) = aA_i t^{-m_i} e^{-k_i t}$$
 (2)

$$P_i(t) = aA_i t^{-m_i} (3)$$

Jump distribution analysis of each of the three PNC systems shows a significant fall in the peak counts for one-frame jump of large amplitude in AA-PNC compared to UN or BA-PNCs, whereas the fwhm of the Gaussian fit showed AA-PNC to be broader (Figure 5b).⁴⁶ This can be attributed to the large fluctuation of ON-state intensities, which contributed to the higher counts of lower amplitude one-frame jumps. ONfraction analysis, i.e., fraction of events lying above the ONstate threshold mentioned above for 76 particles of each, Un-PNCs, BA-PNCs, and AA-PNCs were extracted, and their distribution is shown in Figure 5c. Statistical analysis shows the consistency of trend for all PNCs as observed in the representative timetraces in Figure 4 above, i.e., the passivation has improved emissive quality to mostly ON type. ON-fraction histograms for each PNC were fitted with the Gaussian function to extract their distribution mean and standard deviation as shown in the inset table of Figure 5c. The peaks and SD of 0.58 and 0.29 for Un-PNCs improved to 0.74 and 0.15 for BA-PNCs and further to 0.85 and 0.16 for AA-PNCs (Table 2).

Table 2. Gaussian Fitting Parameters of the Histogram

samples	fresh mean (x_c)	fresh SD (w)	old mean (x_c)	old SD (w)
Un-PNC	0.5832	0.2979	0.4004	0.1337
BA-PNC	0.7352	0.1454	0.6655	0.1718
AA-PNC	0.8460	0.1641	0.7687	0.1525

To check long-term stability, we performed SP PL intermittency study on 50 particles for each PNC that was stored in colloidal form for 4 months. Three representative timetraces are shown in Figure 5d, and other timetraces (10 for each PNC system) are shown in Figure S13. Statistical ONfraction extracted for these particles are given in Figure 5e. Gaussian fitting performed (eq 4) for each PNC system and Table 2 show that their mean and SD of ON-fractions to Un-PNCs decreased from 0.58 to 0.40. In contrast, passivated AA-PNCs and BA-PNCs showed only a decrease from 0.84 to 0.77 and 0.74 to 0.66, respectively, with a narrower distribution. These results demonstrate that AA-PNCs and BA-PNCs showed better long-term stability compared with Un-PNCs.

$$y = y_0 + \frac{A}{w\sqrt{\pi/2}}e^{-2(x-x_c)^2/w^2}$$
(4)

We further performed SPPL lifetime measurements to understand the nature of the traps involved in the PL intermittency study. We used a 485 nm pulsed laser for this study. The PL timetraces showed no significant difference from that of 405 nm excitation, with Un-PNCs exhibiting mostly

'Blinking Up' and 'Frequently Blinking' type intermittency, and passivated PNCs showing a switch toward "Blinking Down" like intermittency. Figure 6a,d,g shows the overlay traces of temporal PL intensity and lifetime for Un-PNC, BA-PNC, and AA-PNC, respectively. The perfect overlap is indicative of either type-A or type-C blinking involving either deep or/and shallow traps, respectively, and not HC blinking (type-B). 47 To further identify the nature of traps involved, PL decay traces at different intensity levels were extracted and are shown in Figure 6b,e,h. PL decay curves from the region of interest are marked with a box of the same color. All three PNCs show a monoexponential decay indicative of two important properties. First, it indicates that timetraces are extracted from SPs as a monoexponential decay profile emanating from multiple particles simultaneously in the ON-state (or at different intensity levels) having the same exciton lifetime is improbable.⁴⁸ Second, the OFF-state decay profile for all three systems also shows monoexponential decay with $t_{\rm off} > 4.0$ ns suggestive of NR type-C blinking via NBC shallow traps. Further, the intensity-lifetime scaling value η = 1.07, 1.16, and 0.98 (calculated from eq 5) for Un, BA, and AA-PNC being less than 2.0 indicates no contribution from the Auger recombination process. 48 Further, the fluorescence lifetime intensity distribution (FLID) scatter plot between PL and average lifetime shows a linear correlation (Figure 6c,f,i for Un-PNC, BA-PNC, and AA-PNC, respectively) which suggests the presence of shallow traps, with AA-PNCs having either less number of traps or they stay mostly inactive delivering a strong temporal PL activity with mostly ON type temporal emission.

$$\eta = \frac{I_{\rm ON}}{\tau_{\rm ON}} : \frac{\tau_{\rm OFF/Grey}}{I_{\rm OFF/Grey}} \tag{5}$$

2.4. Rationalization of SP Blinking Data: Correlation with Bulk. Here, in this study, we observe that both AA and BA show almost similar levels of passivation, as confirmed by the reduced trapping characteristics in TA spectroscopy. However, in the SP blinking study, we observed that AA passivation reduced the OFF-state contribution more efficiently than BA. The PL blinking characteristics are directly correlated with the nature and distribution density of trap states, suggesting that AA passivates the trap of Un-PNC more effectively than BA. This indicates a clear difference in the results of trap passivation between the bulk and the SP level. One key point is that the TA experiment, TRPL experiments, and SP blinking are performed with different levels of dilution of the NCs. Very recently, Gallagher et al. have shown how the effect of dilution on ligand desorption from the NC surface is influenced by the dynamic binding of OA/OAm.²⁴ So, to address the anomaly between the TA experiment and SP blinking of the NCs, the effect of dilution on carrier dynamics was probed through TRPL (Figure 7a-c). For Un-PNC and the BA- and AA-treated NCs, we have taken two sets of dilutions; one that is used for the steady-state PLQY experiment, and another one that is 1000 times more diluted than the samples used for PLQY measurements. At the PLQY concentration, as discussed earlier in Figure 1b, the stretched lifetime and the corresponding stretched exponent value of Un-PNC are 5.3 ns and 0.64,ns, respectively (Figure 7a and Table S1). After \sim 1000 times dilution, the Un-PNC lifetime is decreased to 2.8 ns with a corresponding stretched exponent value of 0.46 (Figure 7a and Table S1). The decrease in the lifetime and the stretched exponent values indicate that the

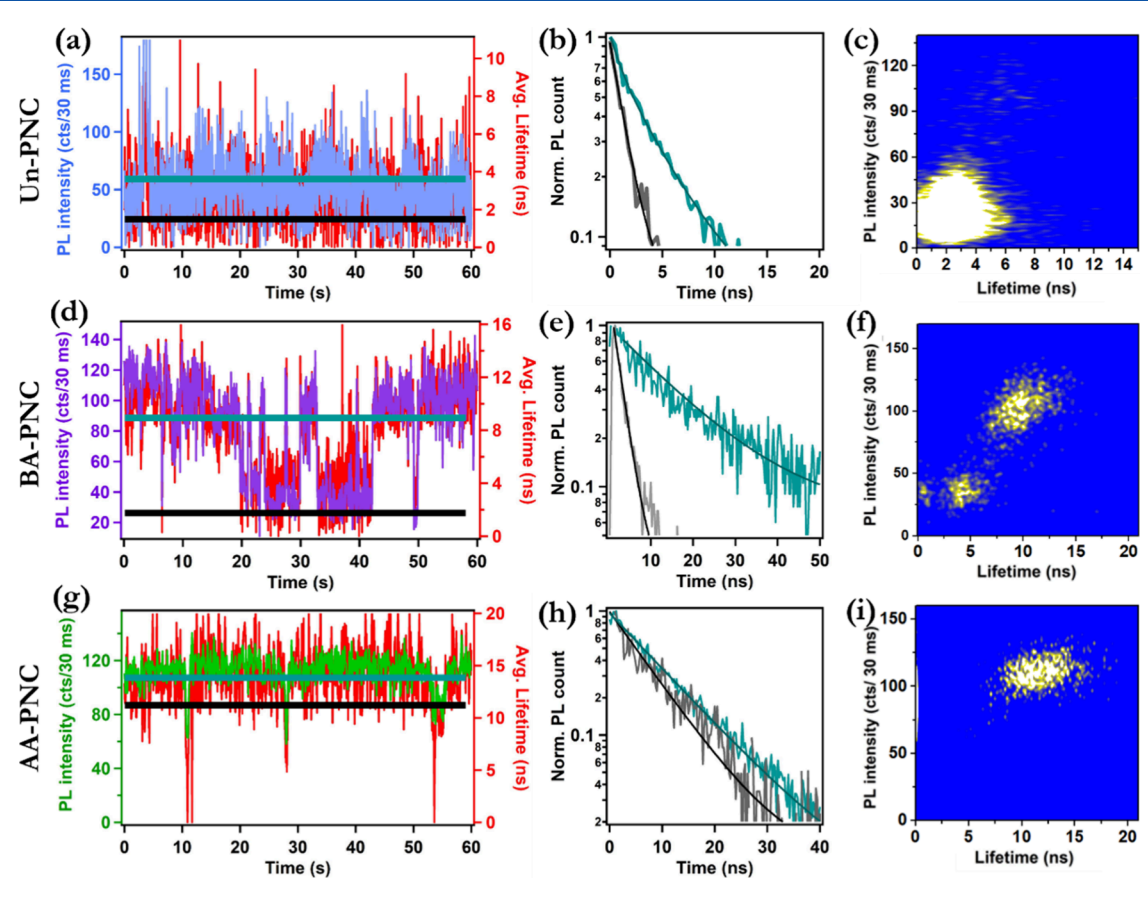


Figure 6. (a) Overlaid plot of PL intensity and average lifetime timetrace, (b) PL decay curve of marked regions (color coded as boxes in a), (c) scattered FLID profile of Un-PNC and (d) overlaid plot for section a of PL intensity and average lifetime timetrace, (e) PL decay curve of marked regions (color coded as boxes in d), (f) scattered FLID profile of BA-PNC, (g) overlaid plot for a section of PL intensity and average lifetime timetrace, (h) PL decay curve of marked regions (color coded as boxes in g), and (i) scattered FLID profile of AA-PNC.

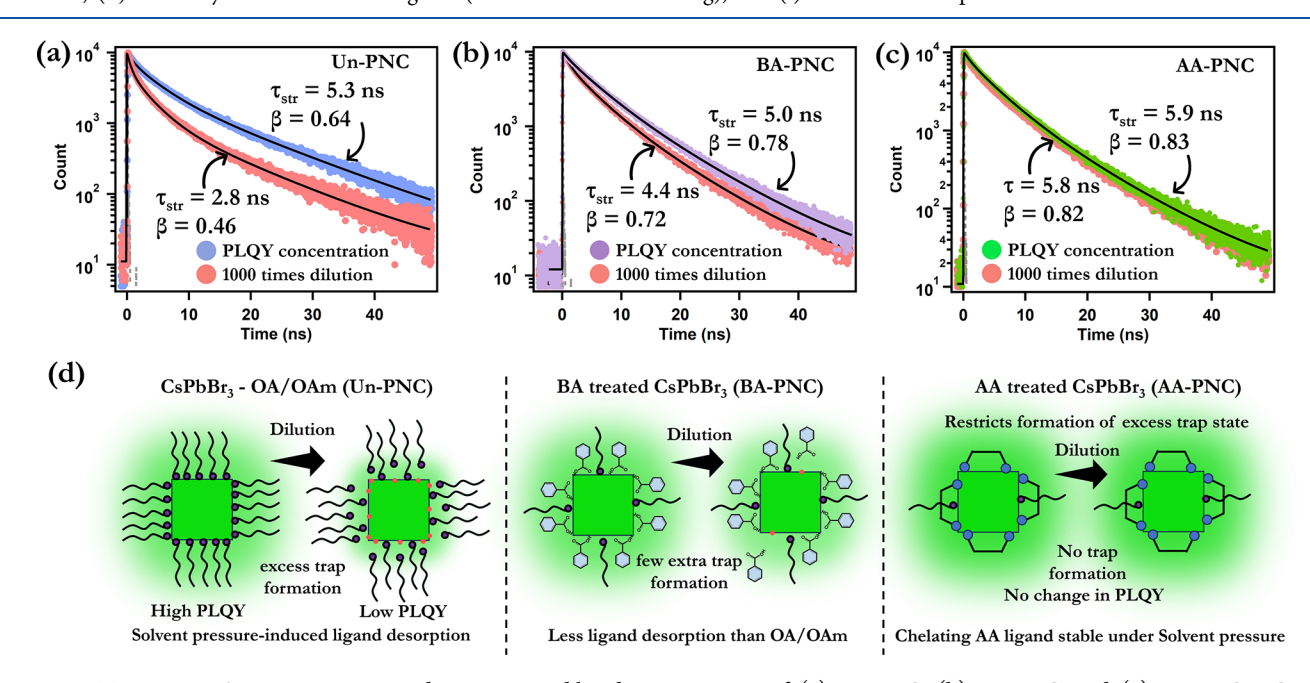


Figure 7. TRPL at PLQY concentration and 1000 times diluted concentration of (a) Un-PNC, (b) BA-PNC, and (c) AA-PNC NCs. (d) Schematic representation of the fate of ligands on the surface of PNCs upon dilution.

dilution severely affected Un-PNC, introducing more trap density on the NC surface. This dilution effect is also seen in BA-PNC where the lifetime is reduced to 4.4 ns from 5.0 ns, and the stretched exponent also changes from 0.78 to 0.72

(Figure 7b and Table S1). The effect of dilution is least observed in the case of AA-PNC where the lifetime and stretched exponent remained almost constant (Figure 7c and Table S1).

This effect can be explained through the solvent-induced desorption of ligands from the PNC surface (Figure 7d). Because of the dynamic ligand binding of OA/OAm, Un-PNC experiences the most adverse effect with the formation of surface traps originating from the dilution-induced ligand desorption. The treatment with short-chain acids offers a much stronger binding to the NC surface and eventually minimizes the dilution-induced ligand loss, as evident from Figure 7b,c. BA-PNC also experiences ligand loss upon dilution, but the effect is much lower than that of Un-PNC (Figure 7a,b). However, AA provides the most effective binding to the PNC surface and virtually eliminates ligand loss when diluted (Figure 7c), indicating a much stronger binding with the PNC surface compared to BA molecules.

Indeed, our DFT studies show that the adsorption energy for the AA system is -1.28 eV, significantly lower than that of the BA system (-0.61 eV). This suggests that AA molecules exhibit stronger adsorption on the PNC surface than BA molecules (Figure 8a). We perform charge density difference

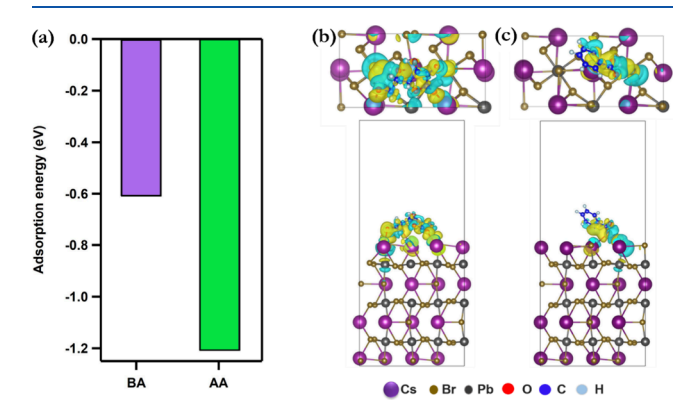


Figure 8. (a) Comparative adsorption energy of BA and AA on the $CsPbBr_3$ surface. Top and side views of the charge density difference for the (b) AA system and (c) BA system. Yellow and cyan regions represent electron accumulation and depletion, respectively, with an isosurface value of 0.0003 e/ų.

analysis to further investigate charge redistribution upon adsorption, as shown in Figure 8b,c. In both cases, charge accumulation occurs near the adsorbed molecules, while charge depletion is observed on the slab surface. However, the interaction of three atoms with Cs in the AA system led to a more pronounced charge accumulation within the molecule. This also hints at the chelating binding of AA molecules to the PNC surface. In contrast, only a single oxygen atom forms a bond with Cs for the BA system, resulting in a weaker adsorption. Consequently, the AA molecule binds more strongly to the perovskite surface than the BA molecule, preventing the formation of surface traps due to dilutioninduced ligand detachment. We selected the CsBr-terminated (100) surface based on extensive literature evidence, identifying this termination as the most energetically favorable and structurally stable for cubic CsPbBr3 perovskites. Numerous experimental and first-principles DFT studies have systematically compared various surface terminations and consistently reported that the charge-neutral CsBr termination exhibits the lowest surface formation energy.^{49–51} For example, models employing PbBr₂ termination generally show poorer agreement with experimental observations compared with CsBr-terminated models. Consequently, the CsBr-terminated (100) surface is widely regarded as the most

representative configuration for modeling stoichiometric, well-crystallized NCs. ^{49,50} Therefore, for a generalized study not tied to a specific nonstoichiometric synthesis protocol, modeling the most stable surface provides a robust understanding of the fundamental properties.

3. CONCLUSIONS

In conclusion, this study provides detailed insight into the effect of AA and BA treatments on the charge carrier dynamics of CsPbBr₃ NCs from the ensemble average to the SP level. The ensemble average picture of carrier dynamics from TA spectroscopy reveals the effective passivation of surface traps upon treatment with AA and BA, also reflected in enhanced PLQY and PL lifetime. However, this postsynthetic small acid treatment on CsPbBr3 does not show any prominent effect on the HC cooling and biexciton dynamics. This effect of trap passivation is also reflected in the temporal SPPL behavior of the NCs. The temporal SPPL fluctuation of Un-PNC is found to be governed by the shallow trap-mediated NBC blinking mechanism. The surface trap passivation by AA and BA significantly reduced the SPPL fluctuation with significant enhancement in the ON-fraction from 0.61 in Un-PNC to 0.74 and 0.84 in BA-PNC and AA-PNC, respectively. The ensemble average picture of charge-carrier trapping in Un-PNC was reduced to a similar extent through postsynthetic treatment, with both AA and BA estimated through GSB recovery in TA spectroscopy. However, the improvement in the temporal SPPL activity of BA-PNC was shadowed by AA-PNC. This anomaly was found to have originated from the dilutioninduced ligand desorption from the NC surface, which was confirmed through TRPL analysis. This dilution effect was found most severe in the case of Un-PNC mainly because of the dynamic capping of the OA/OAm ligand pair. The extent of ligand desorption upon dilution for BA-PNC is much less than that for Un-PNC but not negligible. However, the AA-PNC shows no such ligand loss upon dilution because of the strong chelating interaction with the NC surface. This strong chelating effect of AA is also reflected in almost unchanged ON-fraction even after 4 months of storage. This particular effect of ligand desorption was found to be responsible for the difference in temporal PL fluctuations between AA-PNC and BA-PNC at the SP level. Most of the PL blinking studies in the literature involving pristine CsPbBr₃ NCs show temporal PL fluctuation with a large OFF-fraction. Theoretical simulation performed using DFT study showed that the binding energy of AA to the CsPbBr₃ surface (-1.28 eV) is significantly more negative than that of BA (-0.61 eV), thus able to passivate the Cs vacancy traps on the PNC surface. This higher binding energy of AA is directly associated with ligand loss, which remains unaffected during the dilution process. This study indicates that the dilution may have an unavoidable effect on PL blinking characteristics which should be considered with importance. By protecting the dilution-induced excited-state heterogeneity with AA, this study also shows that we may generate long-term stable blinking-suppressed PNCs without compromising facile charge-transfer ability, opening the door to be studied in developing efficient LED and single-emitter

ASSOCIATED CONTENT

Supporting Information

The Supporting Information is available free of charge at https://pubs.acs.org/doi/10.1021/acsanm.5c03206.

Experimental section, materials and methods, synthesis of CsPbBr3 NCs and post synthetic modification with AA and BA treatments, TEM and PXRD, TA spectral analysis, computational analysis method, SP analysis, characterization and instrumentation, characterization figure, schematic of our confocal microscope setup used to study SP, emission spectra and timetraces of all individuals of all three PNCs, and more results and discussion (PDF)

AUTHOR INFORMATION

Corresponding Authors

Saumyakanti Khatua — Department of Chemistry, Indian Institute of Technology-Gandhinagar, Gandhinagar, Gujarat 382355, India; orcid.org/0000-0002-8088-2132; Email: khatuask@iitgn.ac.in

Nimai Mishra — Institute of Chemical Technology Mumbai, Indian Oil Odisha Campus Bhubaneswar, IIT Kharagpur Extension Center, Bhubaneswar, Odisha 751013, India; orcid.org/0000-0002-6768-1539; Email: n.mishra@iocb.ictmumbai.edu.in

Authors

N. V. S. Praneeth — Department of Chemistry, Indian Institute of Technology-Gandhinagar, Gandhinagar, Gujarat 382355, India; orcid.org/0000-0001-9781-3355

Shovon Chatterjee — Institute of Chemical Technology Mumbai, Indian Oil Odisha Campus Bhubaneswar, IIT Kharagpur Extension Center, Bhubaneswar, Odisha 751013, India; © orcid.org/0000-0002-4136-624X

Subarna Biswas – Institute of Chemical Technology Mumbai, Indian Oil Odisha Campus Bhubaneswar, IIT Kharagpur Extension Center, Bhubaneswar, Odisha 751013, India

Amitrajit Mukherjee – Molecular Imaging and Photonics, Department of Chemistry, KU Leuven, 3001 Leuven, Belgium

Ram Sewak – Department of Chemistry, Indian Institute of Technology-Gandhinagar, Gandhinagar, Gujarat 382355, India; oorcid.org/0000-0001-5700-0122

Abhijit Dutta — Department of Chemistry, Indian Institute of Technology Kanpur, Kanpur 208016, India; ● orcid.org/0009-0002-1409-9593

Anirban Mondal — Department of Chemistry, Indian Institute of Technology-Gandhinagar, Gandhinagar, Gujarat 382355, India; ocid.org/0000-0003-3029-8840

Complete contact information is available at: https://pubs.acs.org/10.1021/acsanm.5c03206

Author Contributions

*N.V.S.P. and S.C. contributed equally to this work.

The authors declare no competing financial interest.

ACKNOWLEDGMENTS

We acknowledge financial support from the Science and Engineering Research Board, India (project numbers: CRG/2020/003471, CRG/2022/005380, TAR/2018/000732, and PDF/2023/000211). S.C. thanks the National Postdoctoral Fellowship (PDF/2023/000211) for providing postdoctoral fellowship support. A.D. acknowledges the Council of Scientific & Industrial Research (CSIR) for providing the graduate fellowship. We sincerely acknowledge Prof. Pratik Sen of IIT Kanpur for helping with the TA facility.

REFERENCES

- (1) Dey, A.; Ye, J.; De, A.; Debroye, E.; Ha, S. K.; Bladt, E.; Kshirsagar, A. S.; Wang, Z.; Yin, J.; Wang, Y.; Quan, L. N.; Yan, F.; Gao, M.; Li, X.; Shamsi, J.; Debnath, T.; Cao, M.; Scheel, M. A.; Kumar, S.; Steele, J. A.; Gerhard, M.; Chouhan, L.; Xu, K.; Wu, X.; Li, Y.; Zhang, Y.; Dutta, A.; Han, C.; Vincon, I.; Rogach, A. L.; Nag, A.; Samanta, A.; Korgel, B. A.; Shih, C.-J.; Gamelin, D. R.; Son, D. H.; Zeng, H.; Zhong, H.; Sun, H.; Demir, H. V.; Scheblykin, I. G.; Mora-Seró, I.; Stolarczyk, J. K.; Zhang, J. Z.; Feldmann, J.; Hofkens, J.; Luther, J. M.; Pérez-Prieto, J.; Li, L.; Manna, L.; Bodnarchuk, M. I.; Kovalenko, M. V.; Roeffaers, M. B. J.; Pradhan, N.; Mohammed, O. F.; Bakr, O. M.; Yang, P.; Müller-Buschbaum, P.; Kamat, P. V.; Bao, Q.; Zhang, Q.; Krahne, R.; Galian, R. E.; Stranks, S. D.; Bals, S.; Biju, V.; Tisdale, W. A.; Yan, Y.; Hoye, R. L. Z.; Polavarapu, L. State of the Art and Prospects for Halide Perovskite Nanocrystals. ACS Nano 2021, 15 (7), 10775–10981.
- (2) Ketavath, R.; Mohan, L.; Sumukam, R. R.; Alsulami, Q. A.; Premalatha, A.; Murali, B. Can Perovskites Be Efficient Photocatalysts in Organic Transformations? *J. Mater. Chem. A Mater.* **2022**, *10* (23), 12317–12333.
- (3) Datta, S.; Mitra, M.; Roy, S. HPMC-Mediated ZnCl ₂ Doping Possible Substitution of Pb ²⁺ for Environment-Friendly Halide Perovskite Solar Cell Fabrication. *ECS Journal of Solid State Science and Technology* **2023**, 12 (10), 105005.
- (4) Kovalenko, M. V.; Protesescu, L.; Bodnarchuk, M. I. Properties and Potential Optoelectronic Applications of Lead Halide Perovskite Nanocrystals. *Science* **2017**, *358* (6364), 745–750.
- (5) Kumawat, N. K.; Swarnkar, A.; Nag, A.; Kabra, D. Ligand Engineering to Improve the Luminance Efficiency of CsPbBr ₃ Nanocrystal Based Light-Emitting Diodes. *J. Phys. Chem. C* **2018**, 122 (25), 13767–13773.
- (6) Fiuza-Maneiro, N.; Sun, K.; López-Fernández, I.; Gómez-Graña, S.; Müller-Buschbaum, P.; Polavarapu, L. Ligand Chemistry of Inorganic Lead Halide Perovskite Nanocrystals. *ACS Energy Lett.* **2023**, 8 (2), 1152–1191.
- (7) Haydous, F.; Gardner, J. M.; Cappel, U. B. The Impact of Ligands on the Synthesis and Application of Metal Halide Perovskite Nanocrystals. *J. Mater. Chem. A* **2021**, *9* (41), 23419–23443.
- (8) Otero-Martínez, C.; Fiuza-Maneiro, N.; Polavarapu, L. Enhancing the Intrinsic and Extrinsic Stability of Halide Perovskite Nanocrystals for Efficient and Durable Optoelectronics. *ACS Appl. Mater. Interfaces* **2022**, *14* (30), 34291–34302.
- (9) Wang, Y.; Ren, Y.; Zhang, S.; Wu, J.; Song, J.; Li, X.; Xu, J.; Sow, C. H.; Zeng, H.; Sun, H. Switching Excitonic Recombination and Carrier Trapping in Cesium Lead Halide Perovskites by Air. *Commun. Phys.* **2018**, *1* (1), 96.
- (10) Zheng, C.; Wang, W.; Xu, L.; Xiang, X.; Liu, W.; Chen, B. Boosting the Carrier Lifetime and Optical Activity of CsPbX ₃ Nanocrystals through Aromatic Ligand Passivation. *J. Phys. Chem. Lett.* **2024**, *15* (17), 4633–4639.
- (11) Paul, S.; Ahmed, T.; Das, S.; Samanta, A. Effect of Lead: Halide Precursor Ratio on the Photoluminescence and Carrier Dynamics of Violet- and Blue-Emitting Lead Halide Perovskite Nanocrystals. *J. Phys. Chem. C* **2021**, *125* (42), 23539–23547.
- (12) Kim, T.; Jung, S. I.; Ham, S.; Chung, H.; Kim, D. Elucidation of Photoluminescence Blinking Mechanism and Multiexciton Dynamics in Hybrid Organic—Inorganic Perovskite Quantum Dots. *Small* **2019**, *15* (33), No. e1900355.
- (13) Hong, D.; Zhang, Y.; Pan, S.; Liu, H.; Mao, W.; Lu, Z.; Tian, Y. Moisture-Dependent Blinking of Individual CsPbBr ₃ Nanocrystals Revealed by Single-Particle Spectroscopy. *J. Phys. Chem. Lett.* **2022**, *13* (46), 10751–10758.
- (14) Swarnkar, A.; Chulliyil, R.; Ravi, V. K.; Irfanullah, M.; Chowdhury, A.; Nag, A. Colloidal CsPbBr ₃ Perovskite Nanocrystals: Luminescence beyond Traditional Quantum Dots. *Angew. Chem.* **2015**, *127* (51), 15644–15648.
- (15) Mi, C.; Gee, G. C.; Lander, C. W.; Shin, D.; Atteberry, M. L.; Akhmedov, N. G.; Hidayatova, L.; DiCenso, J. D.; Yip, W. T.; Chen,

- B.; Shao, Y.; Dong, Y. Towards Non-Blinking and Photostable Perovskite Quantum Dots. *Nat. Commun.* **2025**, *16* (1), 204.
- (16) Ahmed, T.; Seth, S.; Samanta, A. Mechanistic Investigation of the Defect Activity Contributing to the Photoluminescence Blinking of CsPbBr ₃ Perovskite Nanocrystals. *ACS Nano* **2019**, *13* (11), 13537–13544.
- (17) Yarita, N.; Tahara, H.; Saruyama, M.; Kawawaki, T.; Sato, R.; Teranishi, T.; Kanemitsu, Y. Impact of Postsynthetic Surface Modification on Photoluminescence Intermittency in Formamidinium Lead Bromide Perovskite Nanocrystals. *J. Phys. Chem. Lett.* **2017**, 8 (24), 6041–6047.
- (18) Seth, S.; Ahmed, T.; Samanta, A. Photoluminescence Flickering and Blinking of Single CsPbBr ₃ Perovskite Nanocrystals: Revealing Explicit Carrier Recombination Dynamics. *J. Phys. Chem. Lett.* **2018**, 9 (24), 7007–7014.
- (19) Singha, P. K.; Mukhopadhyay, T.; Tarif, E.; Ali, F.; Datta, A. Competition among Recombination Pathways in Single FAPbBr3 Nanocrystals. *J. Chem. Phys.* **2024**, *161* (5), No. 054704.
- (20) Takagi, T.; Omagari, S.; Vacha, M. Suppression of Blinking in Single CsPbBr ₃ Perovskite Nanocrystals through Surface Ligand Exchange. *Phys. Chem. Chem. Phys.* **2023**, 25 (28), 19004–19012.
- (21) Yao, J.-S.; Zhang, J.-C.; Wang, L.; Wang, K.-H.; Ru, X.-C.; Yang, J.-N.; Wang, J.-J.; Chen, X.; Song, Y.-H.; Yin, Y.-C.; Lan, Y.-F.; Zhang, Q.; Yao, H.-B. Suppressing Auger Recombination in Cesium Lead Bromide Perovskite Nanocrystal Film for Bright Light-Emitting Diodes. *J. Phys. Chem. Lett.* **2020**, *11* (21), 9371–9378.
- (22) Jin, H.; Mukherjee, A.; Chouhan, L.; Steele, J. A.; de Jong, F.; Gao, Y.; Roeffaers, M. B. J.; Hofkens, J.; Debroye, E. Single-Particle Optical Study on the Effect of Chloride Post-Treatment of MAPbI 3 Nano/Microcrystals. *Nanoscale* **2023**, *15* (11), 5437–5447.
- (23) Zhang, B.; Goldoni, L.; Zito, J.; Dang, Z.; Almeida, G.; Zaccaria, F.; de Wit, J.; Infante, I.; De Trizio, L.; Manna, L. Alkyl Phosphonic Acids Deliver CsPbBr ₃ Nanocrystals with High Photoluminescence Quantum Yield and Truncated Octahedron Shape. *Chem. Mater.* **2019**, *31* (21), 9140–9147.
- (24) Gallagher, S.; Kline, J.; Jahanbakhshi, F.; Sadighian, J. C.; Lyons, I.; Shen, G.; Hammel, B. F.; Yazdi, S.; Dukovic, G.; Rappe, A. M.; Ginger, D. S. Ligand Equilibrium Influences Photoluminescence Blinking in CsPbBr 3: A Change Point Analysis of Widefield Imaging Data. ACS Nano 2024, 18 (29), 19208–19219.
- (25) Dutt, V. G. V.; Akhil, S.; Singh, R.; Palabathuni, M.; Mishra, N. Year-Long Stability and Near-Unity Photoluminescence Quantum Yield of CsPbBr ₃ Perovskite Nanocrystals by Benzoic Acid Post-Treatment. *J. Phys. Chem. C* **2022**, *126* (22), 9502–9508.
- (26) Dutt, V. G. V.; Akhil, S.; Singh, R.; Palabathuni, M.; Mishra, N. High-Quality CsPbX ₃ (X = Cl, Br, or I) Perovskite Nanocrystals Using Ascorbic Acid Post-Treatment: Implications for Light-Emitting Applications. *ACS Appl. Nano Mater.* **2022**, *5* (5), 5972–5982.
- (27) Biswas, S.; Akhil, S.; Kumar, N.; Palabathuni, M.; Singh, R.; Dutt, V. G. V.; Mishra, N. Exploring the Role of Short Chain Acids as Surface Ligands in Photoinduced Charge Transfer Dynamics from CsPbBr ₃ Perovskite Nanocrystals. *J. Phys. Chem. Lett.* **2023**, *14* (7), 1910–1917.
- (28) Kresse, G.; Joubert, D. From Ultrasoft Pseudopotentials to the Projector Augmented-Wave Method. *Phys. Rev. B* **1999**, *59* (3), 1758–1775.
- (29) Kresse, G.; Hafner, J. Ab Initio Molecular-Dynamics Simulation of the Liquid-Metal—Amorphous-Semiconductor Transition in Germanium. *Phys. Rev. B* **1994**, *49* (20), 14251–14269.
- (30) Fisher, B. R.; Eisler, H.-J.; Stott, N. E.; Bawendi, M. G. Emission Intensity Dependence and Single-Exponential Behavior In Single Colloidal Quantum Dot Fluorescence Lifetimes. *J. Phys. Chem. B* **2004**, *108*, 143–148.
- (31) Teunis, M. B.; Johnson, M. A.; Muhoberac, B. B.; Seifert, S.; Sardar, R. Programmable Colloidal Approach to Hierarchical Structures of Methylammonium Lead Bromide Perovskite Nanocrystals with Bright Photoluminescent Properties. *Chem. Mater.* **2017**, 29 (8), 3526–3537.

- (32) van Driel, A. F.; Nikolaev, I. S.; Vergeer, P.; Lodahl, P.; Vanmaekelbergh, D.; Vos, W. L. Statistical Analysis of Time-Resolved Emission from Ensembles of Semiconductor Quantum Dots: Interpretation of Exponential Decay Models. *Phys. Rev. B* **2007**, *75* (3), No. 035329.
- (33) Chatterjee, S.; Sen, A.; Sen, P. Green Synthesis of 3D Cesium Lead Halide Perovskite Nanocrystals and 2D Ruddlesden-Popper Nanoplatelets in Menthol-Based Deep Eutectic Solvents. *Mater. Chem. Front* **2023**, 7 (4), 753–764.
- (34) Mondal, N.; De, A.; Das, S.; Paul, S.; Samanta, A. Ultrafast Carrier Dynamics of Metal Halide Perovskite Nanocrystals and Perovskite-Composites. *Nanoscale* **2019**, *11* (20), 9796–9818.
- (35) Chatterjee, S.; Mukhopadhyay, A.; Mondal, S.; Sourav, S.; Bhowmik, S.; Goswami, N.; Mishra, N. Hot Carrier Transfer from CsPbBr3 Nanocrystal to Au25 Cluster: The Pivotal Role of Ligand-Controlled Diffusion. *Nanoscale* **2025**, *17*, 22905.
- (36) Ghosh, G.; Marjit, K.; Ghosh, S.; Patra, A. Hot Carrier Cooling and Biexciton Dynamics of Anisotropic-Shaped CsPbBr ₃ Perovskite Nanocrystals. *J. Phys. Chem. C* **2023**, *127* (18), 8670–8679.
- (37) Mukherjee, S.; Ghosh, S.; Ghosal, M.; Dey, S.; Mandal, S.; De, C. K.; Debnath, R.; Karmakar, M.; Karmakar, A. J.; Datta, P. K.; Mandal, P. K. Super-Absorber, Super-Bright, Nearly-Non-Blinking CsPbI ₃ Perovskite Nanocrystal. *Adv. Opt. Mater.* **2025**, *13*, No. 2402608.
- (38) Ye, J.; Mondal, N.; Carwithen, B. P.; Zhang, Y.; Dai, L.; Fan, X.-B.; Mao, J.; Cui, Z.; Ghosh, P.; Otero-Martínez, C.; van Turnhout, L.; Huang, Y.-T.; Yu, Z.; Chen, Z.; Greenham, N. C.; Stranks, S. D.; Polavarapu, L.; Bakulin, A.; Rao, A.; Hoye, R. L. Z. Extending the Defect Tolerance of Halide Perovskite Nanocrystals to Hot Carrier Cooling Dynamics. *Nat. Commun.* **2024**, *15* (1), 8120.
- (39) Das, A.; Marjit, K.; Ghosh, S.; Ghosh, D.; Patra, A. Slowing Down the Hot Carrier Relaxation Dynamics of CsPbX ₃ Nanocrystals by the Surface Passivation Strategy. *J. Phys. Chem. C* **2023**, *127* (31), 15385–15394.
- (40) Makarov, N. S.; Guo, S.; Isaienko, O.; Liu, W.; Robel, I.; Klimov, V. I. Spectral and Dynamical Properties of Single Excitons, Biexcitons, and Trions in Cesium—Lead-Halide Perovskite Quantum Dots. *Nano Lett.* **2016**, *16* (4), 2349—2362.
- (41) Aneesh, J.; Swarnkar, A.; Kumar Ravi, V.; Sharma, R.; Nag, A.; Adarsh, K. V. Ultrafast Exciton Dynamics in Colloidal CsPbBr ₃ Perovskite Nanocrystals: Biexciton Effect and Auger Recombination. *J. Phys. Chem. C* **2017**, *121* (8), 4734–4739.
- (42) Lv, Y.; Duan, M.; An, J.; Wang, Y.; Du, L. Ultrafast Study of Interfacial Charge Transfer Mechanism in Assembled Systems of CsPbBr 3 and Titanium Dioxide: Size Effect of CsPbBr3. *Nanomaterials* **2025**, *15* (14), 1065.
- (43) Chen, R.; Xia, B.; Zhou, W.; Zhang, G.; Qin, C.; Hu, J.; Scheblykin, I. G.; Xiao, L. Environment-Dependent Metastable Nonradiative Recombination Centers in Perovskites Revealed by Photoluminescence Blinking. *Adv. Photonics Res.* **2022**, 3 (1), No. 2100271.
- (44) Mukherjee, A.; Ray, K. K.; Phadnis, C.; Layek, A.; Bera, S.; Chowdhury, A. Insights on Heterogeneity in Blinking Mechanisms and Non-Ergodicity Using Sub-Ensemble Statistical Analysis of Single Quantum-Dots. *J. Chem. Phys.* **2019**, *151* (8), No. 084701.
- (45) Kuno, M.; Fromm, D. P.; Hamann, H. F.; Gallagher, A.; Nesbitt, D. J. Nonexponential, "Blinking" Kinetics of Single CdSe Quantum Dots: A Universal Power Law Behavior. *J. Chem. Phys.* **2000**, *112* (7), 3117–3120.
- (46) Pathoor, N.; Halder, A.; Mukherjee, A.; Mahato, J.; Sarkar, S. K.; Chowdhury, A. Fluorescence Blinking Beyond Nanoconfinement: Spatially Synchronous Intermittency of Entire Perovskite Microcrystals. *Angew. Chem., Int. Ed.* **2018**, 57 (36), 11603–11607.
- (47) Galland, C.; Ghosh, Y.; Steinbrück, A.; Sykora, M.; Hollingsworth, J. A.; Klimov, V. I.; Htoon, H. Two Types of Luminescence Blinking Revealed by Spectroelectrochemistry of Single Quantum Dots. *Nature* **2011**, 479 (7372), 203–207.

- (48) Yuan, G.; Gómez, D. E.; Kirkwood, N.; Boldt, K.; Mulvaney, P. Two Mechanisms Determine Quantum Dot Blinking. *ACS Nano* **2018**, *12* (4), 3397–3405.
- (49) Bertolotti, F.; Nedelcu, G.; Vivani, A.; Cervellino, A.; Masciocchi, N.; Guagliardi, A.; Kovalenko, M. V. Crystal Structure, Morphology, and Surface Termination of Cyan-Emissive, Six-Monolayers-Thick CsPbBr 3 Nanoplatelets from X-Ray Total Scattering. ACS Nano 2019, 13 (12), 14294–14307.
- (50) Chen, Y.; Smock, S. R.; Flintgruber, A. H.; Perras, F. A.; Brutchey, R. L.; Rossini, A. J. Surface Termination of CsPbBr ₃ Perovskite Quantum Dots Determined by Solid-State NMR Spectroscopy. *J. Am. Chem. Soc.* **2020**, *142* (13), 6117–6127.
- (51) Ezzeldien, M.; Al-Qaisi, S.; Alrowaili, Z. A.; Alzaid, M.; Maskar, E.; Es-Smairi, A.; Vu, T. V.; Rai, D. P. Electronic and Optical Properties of Bulk and Surface of CsPbBr 3 Inorganic Halide Perovskite a First Principles DFT 1/2 Approach. *Sci. Rep* **2021**, *11* (1), 20622.

